Experiments in Fluids (2006) 40: 405–421
DOI 10.1007/s00348-005-0078-5

RESEARCH ARTICLE

Edward J. Stewart · Pablo Huq

Dissipation rate correction methods

Received: 30 May 2003 / Revised: 20 September 2005 / Accepted: 30 September 2005 / Published online: 3 December 2005

Abstract Dissipation rates of the turbulent kinetic energy and of the scalar variance are underestimated when the measurement resolution of the small scales of a turbulent flow field are insufficient. Results are presented of experiments conducted in a salt-stratified water tunnel (Schmidt number ∼700). Dissipation rates are determined to be underestimated, and thus correction techniques based on velocity structure functions and mixed-moment functions are proposed. Dissipation rates in laboratory experiments of shear-free, grid-generated turbulence are determined from balance calculations of the kinetic energy and scalar variance evolution equations. Comparisons between the structure function and balance estimates of dissipation show that the corrections are O(1) for the kinetic energy dissipation rate, and are O(100) for the scalar variance dissipation rate. This difference is due to the lack of resolution down to the Batchelor scales that is required for a high Schmidt number flow. Simple correction functions based on microscale Reynolds numbers are developed for both turbulent kinetic energy and scalar variance dissipation rates. Application of the technique to the results of laboratory experiments of density stratified turbulence, sheared turbulence, and sheared density stratified turbulence yields successful corrections. It is also demonstrated that the Karman–Howarth equality (and the analogous Yaglom equation) that relates second and third-order structure functions to dissipation rates is valid for both unstrained (decaying grid-generated turbulence) and density stratified and sheared turbulence at least up to the magnitudes of strains of the current experiments Nt∼10, St∼10, respectively. This is helpful for it allows the use of these equations in the analysis of turbulence even when the large scale background profiles of velocity and scalar are unknown.

E. J. Stewart · P. Huq (✉)
College of Marine Studies, University of Delaware,
Newark, DE, 19716 USA
E-mail: huq@udel.edu

1 Introduction and literature review

Dissipation marks the end of the turbulent cascade process. The scale of the smallest (Kolmogorov scale) eddies in a turbulent flow are limited by viscosity. Any energy put into or generated by a turbulent flow at any large (or integral) scale will eventually be dissipated at these smallest scales. Measurement of turbulent dissipation rates is difficult, as it requires resolution of the small scales. Typically, such small scales are not adequately resolved in laboratory experiments. Thus, turbulent dissipation rate estimates can be in error. In this paper, after a review of background information on current techniques used to estimate dissipation rates, methods to correct the measured dissipation rates of turbulent kinetic energy and the scalar variance are each outlined, and examples are provided.

The dissipation rates of both kinetic energy, ε, and scalar, χ, are determined classically in one of four manners. An ideal method would be to measure the dissipation rate directly using the complete definition for the turbulent dissipation rate (i.e., $\varepsilon = \nu \nabla^2 u$ or $\chi = \alpha \nabla^2 \theta$ where ν and α are diffusivities of momentum and scalar). Without using any assumptions for isotropy, this measurement is nearly impossible experimentally as adequate resolution of all spatial gradients in the flow is difficult. However, such measurements are numerically possible [for small values of Prandtl number of O (1)], and results should be verified.

A typical method is to form a surrogate for the full definition of the dissipation rate by substituting one or more of its components. Often, only the longitudinal derivative of velocity or scalar is used (i.e., $\partial u/\partial x$ or $\partial \theta/\partial x$). To account for anisotropy, longitudinal gradients of transverse velocities or transverse gradients of other

velocity components or of the scalar are sometimes used. (Note that, for brevity, both index notation u_i and lower case u are used to designate longitudinal velocity. Thus, for example, u and u_1 is the longitudinal velocity component.)

Thirdly, by measuring or modeling all the terms in the equation governing the evolution of the kinetic energy or of the scalar, one can estimate the change in the turbulent variances due to the dynamics and back out, or balance, the rate at which turbulent kinetic energy, q^2, or scalar fluctuations, θ^2, is dissipated. Such measurements are experimentally difficult due to the fine spatial resolutions required. In addition, other terms such as gradient production are often significant so that the evolution of dq^2/dx or $d\theta^2/dx$ may not be monotonic. However, some flows evolve sufficiently simply to make the method viable. The shear-free isotropic turbulence studied by Comte-Bellot and Corrsin (1966) allowed the energy dissipation rate to be accurately estimated in this manner. By including the shear production term, Harris et al. (1977) were able to estimate the dissipation rate for sheared turbulence using the turbulent kinetic energy evolution equation. Further, Itsweire et al. (1986) used a balance method to evaluate rates of both energy and scalar dissipation rates in an experiment involving stably stratified, shear-free grid turbulence.

Finally, one may estimate a dissipation rate by computing the area under the energy or scalar dissipation spectrum.This method does not require the measurement of every term in the balance equation, but instead requires resolution of the spectrum of velocity or scalar fluctuations. This resolution requires a small probe with a high measurement rate to resolve to the Kolmogorov scales using Taylor's hypothesis; the Kolmogorov lengthscale is defined as $\eta = (\nu^3/\varepsilon)^{1/4}$, where ν is the kinematic viscosity, and ε is the dissipation rate of kinetic energy. To obtain an estimate of scalar dissipation rate in this manner (e.g., of salinity fluctuations in water) would require resolution down to the Batchelor scale $\beta = (\nu D^2/\varepsilon)^{1/4}$ (Batchelor 1959), where D is the diffusivity of salt in water (about 1.4×10^{-5}cm^2/s). For large Prandtl or Schmidt number flows (e.g., heat or salt in water), the resolution of the Batchelor scale proves to be difficult.

The robustness of calculated values of the kinetic energy dissipation rates, ε, and scalar dissipation, χ, depends on the accuracy of turbulent spectra of the respective velocity and scalar fields at small dissipative scales. Values of ε and χ are required to calculate turbulent length scales and to evaluate turbulence evolution. Unfortunately, typical resolutions of velocity and scalar probes are insufficient to fully resolve the turbulent spectra; this usually places severe constraints on accuracy of slopes and range of scales resolved. Therefore, corrections for values of ε and χ are required.

Dissipation rate corrections in the oceanographic literature rely often on "universal forms" of spectra-empirical extensions of the Kolmogorov spectrum down to the dissipative range of wavenumbers (Oakey 1982). This method has limitations, however, as large variations in the inertial sub-range can exist due to site specific generation mechanisms of turbulence. An additional limitation is that buoyancy scaling is often a better fit to data than Kolmogorov scaling (Gregg 1987). Dissipation rates may be estimated by utilizing the Batchelor forms of scalar spectrum (Batchelor 1959; Oakey 1982). This can yield useful estimates of dissipation rates, with the caveat that the technique is "sensitive to the errors in the fit and to the universality of the Batchelor spectrum" (Gregg 1987). A more serious criticism is that the correctness of Batchelor spectral forms for turbulent flows (for both small Prandtl numbers and large Schmidt numbers) have been questioned by the measurements of Gargett (1985), Dowling and Dimotakis 1990) and Miller and Dimotakis (1996).

Many studies have attempted to verify the validity of such dissipation rate calculation methods. Yamazaki and Osborn (1990) include numerous equations defining the dissipation rate through a number of different velocity gradients with various constants. A detailed study by Zhou and Antonia (2000) compares several different methods of estimating both the energy and the scalar dissipation rates. They conclude that regardless of the method used, the refined similarity hypothesis (RSH) of Kolmogorov (1962) is not violated. The proper scaling of the dissipation rate has also been interrogated with experimental data (Sreenivasan 1984) and numerical simulations (Sreenivasan 1998).

Gibson and Masiello (1972) showed that each of the three components of the scalar dissipation rate is of the same magnitude. Sreenivasan et al. (1977) and Danaila et al. (2000) both use four-wire probes (in a turbulent boundary layer and decaying grid-generated turbulence, respectively) to measure the temperature dissipation rate and find a similar conclusion. On the contrary, for stratified turbulence, Thoroddsen and Van Atta (1996) suggest that strong anisotropy in the small scales could contribute to relatively large errors in the estimate of scalar dissipation rate by using only the longitudinal derivative.

2 Experimental setup

2.1 Apparatus

Experiments are conducted using a recirculating water tunnel 400 cm long, 40 cm deep and 25 cm wide with a measurement section 200 cm long. The flow is driven by two pumps which produce a mean velocity in the tunnel of about $U = 7$ cm/s. In order to reduce noise due to

background turbulence, a honeycomb box and a series of mesh screens are placed upstream of the measurement section. Background turbulence intensities of w/U are reduced to 0.3%, where w is the root mean square (rms) vertical velocity fluctuation. Turbulent velocities are laterally homogeneous to within 5% except for boundary layers at the sidewalls of the water tunnel that grew to 2 cm at the furthest downstream location. Water leaving the measurement section is returned to the storage reservoirs and recirculated. The top of the water column possesses a free surface, thus allowing the introduction of probes into the flow. Turbulence is generated in the water tunnel through the introduction of a bi-plane grid. The bi-plane grid comprises square Plexiglas rods with sides of length $d = 0.64$ cm arranged with a mesh of spacing $M = 3.2$ cm, so the ratio of mesh spacing to rod size is $M/d = 5$. Downstream locations are measured from the grid located at $x = 0$ cm. Values of the mesh Reynolds number $\mathrm{Re_M} = UM/v$ are approximately 2,200 for the experiment.

Two reservoirs each feed into initially separate vertical layers of the tunnel (see Fig. 1). Density stratification is affected by adding a brine solution to the reservoir that supplies water to the lower layer. Thus the Schmidt number, the ratio of the diffusivity of momentum to the diffusivity of scalar is 700. A significant linear velocity shear across the middle of the flow field can be generated efficiently using a combination of differential input and exit volumes and a mesh of variable density. Representative vertical density and velocity profiles are shown in Fig. 2. The vertical location z in this figure is scaled by the grid mesh spacing M. Note that the abscissa has two scales and sets of units. The mean density, ρ, is presented in kg/m^3 with values in Fig. 2 shown as the quantity ($\rho - 1{,}000$). The vertical profile of the longitudinal mean velocity is also shown and has units of cm/s. Data were taken at ten longitudinal stations along the centerline of the water tunnel, with ten vertical stations at each location. The vertical extents of linear gradient regions are typically $3M$, which is much greater than integral lengthscales (typically $M/3$). This allows scaling by the density gradient, N, and the velocity gradient, S. There is a large range in values of N and S for the experiments conducted; this leads to a large domain space of Nt and St values (the dimensionless strains used throughout the paper to gauge the importance of stratification and shear). The Brunt-Väisälä frequency, or buoyancy frequency, N is defined as $N = \sqrt{(-g/\rho_0(\mathrm{d}\rho/\mathrm{d}z)}$; the shear frequency S, as $S = \mathrm{d}U/\mathrm{d}z$. Each of these quantities has units of s^{-1}. The dimensionless quantities are constructed using $t = x/U$ yielding $\mathrm{Nt} = \mathrm{Nx}/U$ and $\mathrm{St} = \mathrm{Sx}/U$. Values of Nt and St up to about 9 were attained. Example data sets provided in this paper have been chosen specifically to illustrate the dissipation rate correction technique for a large range of Nt–St space. The first data set is for the case in which the dynamics are similar to decaying grid-generated turbulence, which arises when values of both Nt and St are small. The values in this data set are: $\mathrm{Nt} = 0.3$ and $St = 0.4$. The second data set examines grid generated turbulence in sheared flow, here, $\mathrm{Nt} = 0.5$ and $\mathrm{St} = 4.3$. Representative of shear-free, density stratified flow is the third case which possess values of $\mathrm{Nt} = 4.3$ and $\mathrm{St} = 0.2$. Finally, the fourth case includes the effects of both strong shear and strong stratification, with $\mathrm{Nt} = 4.7$ and $\mathrm{St} = 5.1$.

2.2 Measurements

Concentration measurements are made by an aspirating conductivity probe. The tip of this probe had a 0.2 cm long sensor of 0.1 cm diameter: an orifice of diameter 0.033 cm at the center of the sensor allowed the flow of brine. The spatial resolution of the probe was estimated to be 0.04 cm, and frequency response 70 Hz (see Huq and Britter 1995a for details). A conductivity box controls the probe with an AC bridge driven at 1 kHz. At a given temperature, this probe setup returns a voltage that is a function of only salt concentration. Background noise for this setup is on the order of 5 mV, or about 0.3% of a typical mean. Velocity measurements are obtained using an anemometer with a standard hot-film quartz-coated cylindrical x-probe (TSI type 1241–20 w), which is operated with a 2% overheat ratio. Two perpendicular velocity components

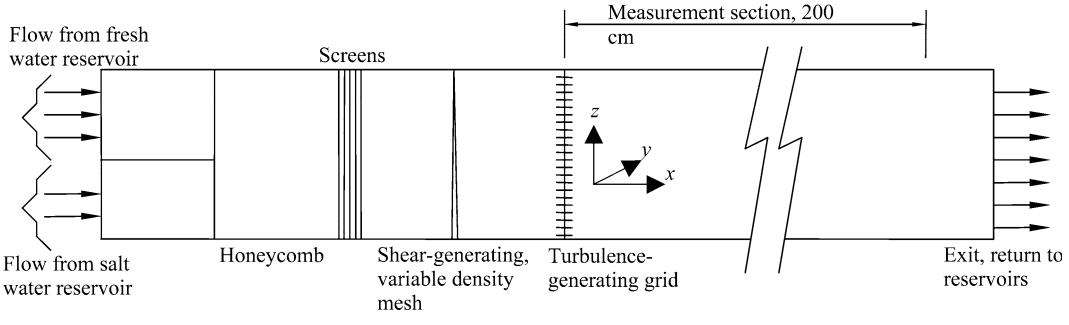

Fig. 1 A schematic of the experimental apparatus. *Arrows* indicate flow entering and leaving the channel. The flow-conditioning honeycomb and screens, the shear generating meshes, and turbulence generating grid are also shown. (Also shown is a coordinate system. Note that $x = 0$ is coincident with the turbulence generating grid)

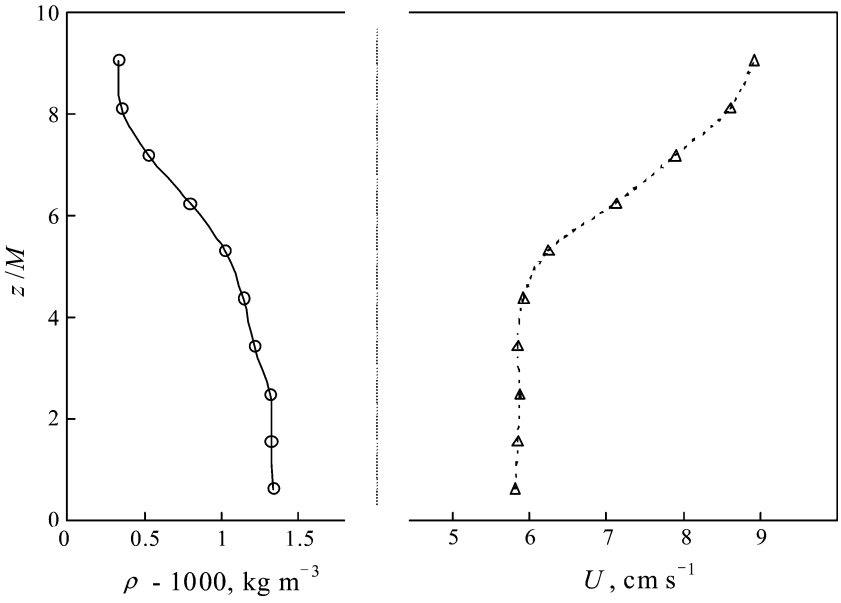

Fig. 2 Sample vertical density and velocity profiles. The vertical location z has been scaled by the turbulence generating grid mesh spacing M. The abscissa is a broken axis of mixed units. The *solid line* is a representative mean density profile $\rho(z)$ in kg/m^3; the *dotted line* is a mean velocity profile $U(z)$ in cm/s. Data taken at $x/M = 40$

are measured simultaneously. A form of King's Law (King 1914) is used to convert voltage output of the anemometer unit to instantaneous velocities. Individual measured velocity components can be computed using the sum and difference method: $u = (V_1 + V_2)/\sqrt{2}$ and $w = (V_1 + V_2)k_y/\sqrt{2}$, where V_1 and V_2 are the effective voltages of either hot wire, u is the longitudinal velocity component, w is the perpendicular component of interest, and $k_y = (1+k^2)/(1 - k^2)$ with $k = 0.35$. This constant is a yaw correction factor used to correct for the small length (0.10 cm) to diameter (0.0051 cm) ratio of about 20 for the hot-film probe (Lawson and Britter 1983). Flux measurements were determined from the simultaneous operation of the x-film and conductivity probes. The conductivity probe was located 0.1 cm from the x-film: the spatial resolution of the flux probe arrangement was estimated to be 0.15 cm. There was no time lag between the velocity and conductivity probes. Typical values of errors in rms fluctuations and correlations were 5 and 10%, respectively.

2.3 Experimental method

Both concentration and velocity data are acquired digitally as voltages by a personal computer. Data are collected at a given point in the flow for at least 30 s at 200 Hz. For the scales of this flow, a typical eddy turnover time is about $l/u' = 3$ s, and so a time series must be at least 30 s in length for frequency spectra to contain ten realizations of this low frequency. Higher order moments require longer time series; thus, in order to evaluate these moments some data sets were collected for up to 200 s. The resulting data sets are long enough to produce reliable higher order moment statistics and are fine enough to resolve the Kolmogorov scales.

Besides being commonly used to estimate dissipation rates, measurements of velocity and scalar derivatives also have implications in the analysis of the small-scale isotropy and intermittency of a turbulent flow. Computation of the derivative is relatively straightforward from Eulerian time series. Choosing a suitable Δt with which to calculate the discrete quantities $\Delta u_i/\Delta t$ and $\Delta \rho/\Delta t$ is a consideration, however. Selection of small values of Δt results in an overly noisy signal with dependence on the response of the probe. If too large a Δt is chosen, the results have physically little to do with the small scales of the flow. For the current data, a $\Delta t = 0.015$ s (or three data points at 200 Hz) was used, which results in a time separation on the order of twice the Kolmogorov scale. This separation has been previously found to yield robust results in derivative computations (e.g., Antonia et al. 1993; Zhou and Antonia 2000), and convergence in the computation of the mean square derivative occurs with this choice of Δt. Employing Taylor's frozen flow hypothesis (Taylor 1938), a Eulerian time series may be examined as a function of the longitudinal spatial coordinate by using the definition $\mathrm{d}x/\mathrm{d}t = U$: $\mathrm{d}u/\mathrm{d}x = (-1/U)(\mathrm{d}u/\mathrm{d}t)$, where U is the local mean longitudinal velocity. From these time series, the further computation of quantities such as $(\mathrm{d}u_i/\mathrm{d}x)^2$ and $(\mathrm{d}\rho/\mathrm{d}x)^2$ is algebraic.

3 Dissipation rate of turbulent kinetic energy

3.1 Definitions

The definition of the energy dissipation rate term in the Reynolds decomposed Navier–Stokes equations for homogeneous steady flow is the nine-term tensor:

$$\varepsilon = \nu \overline{\frac{\partial u_i}{\partial x_j}\frac{\partial u_i}{\partial x_j}} \tag{1}$$

(see for example, Hinze 1975.) The accurate measurement of all nine terms would require an exceptional experimentalist. One of the earliest and most complete measurements was made by Klebanoff (1954) who measured five terms, while assuming isotropic relations to estimate the other four. Another option is to ignore all non-longitudinal derivatives and measure only the three terms $\overline{(\partial u_i/\partial x)^2}$, but these terms are still quite difficult to measure experimentally. The spatial gradients of all three velocity components would necessitate the use of a multiwire hot-film probe. A reduction in the number of velocity components that need to be resolved occurs if one uses the assumption of isotropy at the small scales, thus requiring the measurement of only the longitudinal velocity derivative. This popular surrogate is:

$$\varepsilon = 15\nu\overline{(\partial u/\partial x)^2}, \tag{2}$$

where the constant of 15 arises from isotropy. Hinze (1975) notes that this estimate is generally quite good compared to the Klebanoff (1954) measurements. However, if the flow is anisotropic, the longitudinal derivative may not accurately portray the dissipation rate, and the more complex form of

$$\varepsilon = \nu\left(10\overline{(\partial u/\partial x)^2} + 2.5\overline{(\partial w/\partial x)^2}\right) \tag{3}$$

has been used (e.g., Stillinger et al. 1983). For isotropic flow $\overline{(\partial w/\partial x)^2} = 2\overline{(\partial u/\partial x)^2}$ (see for example, Tavoularis and Corrsin 1981 or Van Atta 1991) and Eq. 3 simplifies to Eq. 2. A comparison of the computation of ε using both Eqs. 2 and 3 is shown in Fig. 3 for the present experiment. The abscissa of this figure is the isotropic surrogate Eq. 2, and the ordinate is the estimate that accounts for small-scale anisotropy, Eq. 3. The diagonal line represents equality between the two estimates. The small scales of the current flow are sufficiently isotropic that using Eq. 3 does not improve the estimate of the dissipation rate, even with significant shear and/or stratification effects at the large scales (with values of Nt and St of up to 9). Thoroddsen (1995) points out that using two probes to measure $\varepsilon = 7.5\nu\overline{(\partial u/\partial z)^2}$ produces similar results to the two equations used above. Yamazaki and Osborn (1990) present a formula for the computation of the dissipation rate based on the two transverse velocity derivatives $\mathrm{d}v/\mathrm{d}x$ and $\mathrm{d}w/\mathrm{d}x$, but Antonia et al. (1986) point out that these derivatives are typically more difficult to measure and including them will yield less accurate results for the dissipation rate.

There is evidence that the scales on which the dissipation occurs are highly correlated with the measured velocity derivative, so the use of the surrogate based only on the mean square longitudinal derivative (Eq. 2) can be briefly justified. For example, the spatial longitudinal derivative $(\mathrm{d}u/\mathrm{d}x)$ is computed with a discrete Δx on the order of the Kolmogorov scale, and it has been suggested that dissipation physically occurs on scales slightly larger than the Kolmogorov lengthscale (Comte-Bellot and Corrsin 1971). Additionally, zero-crossings of the $u(x)$ signal have been found to be well correlated with dissipation events (Kailasnath and Sreenivasan 1993). It is generally at these zero-crossings of $u(x)$ that the magnitude of $(\mathrm{d}u/\mathrm{d}x)^2$ is largest, thus leading to a good physical correlation between the actual dissipation rate and the surrogate of Eq. 2. However, it should be noted that the true dissipation rate and its estimate using $(\mathrm{d}u/\mathrm{d}x)^2$ have different probability density functions (or PDFs) (Tsinober 1993), and are also spectrally different (Bershadskii et al. 1993; Zhou and Antonia 2000). The major difference is that PDFs of

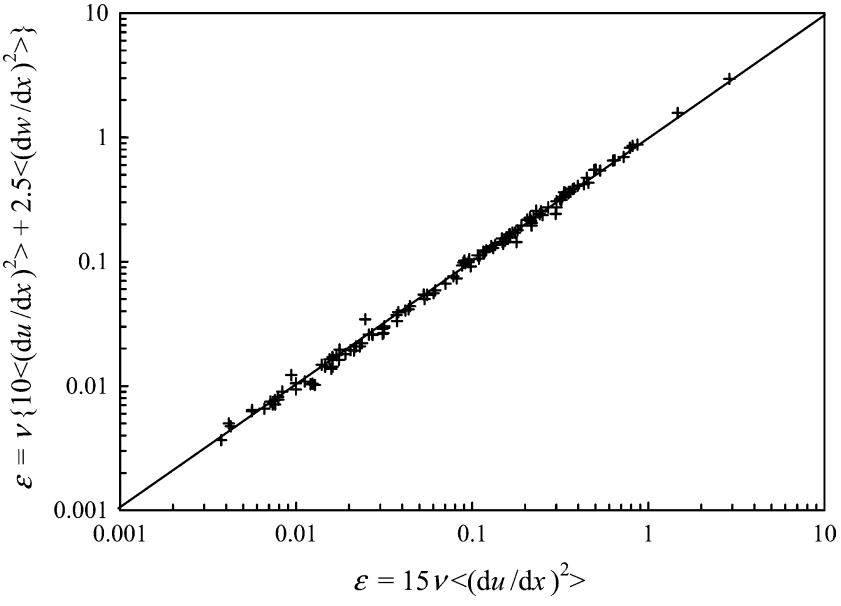

Fig. 3 Comparison of two estimates of turbulent kinetic energy dissipation rate ε. The abscissa is the standard surrogate assuming small-scale isotropy (Eq. 2); the ordinate allows for variation from isotropy explicitly by including the longitudinal derivative of the vertical velocity component (Eq. 3). The line indicates agreement. Data are from the full range of experimental parameters (Nt < 9, St < 9)

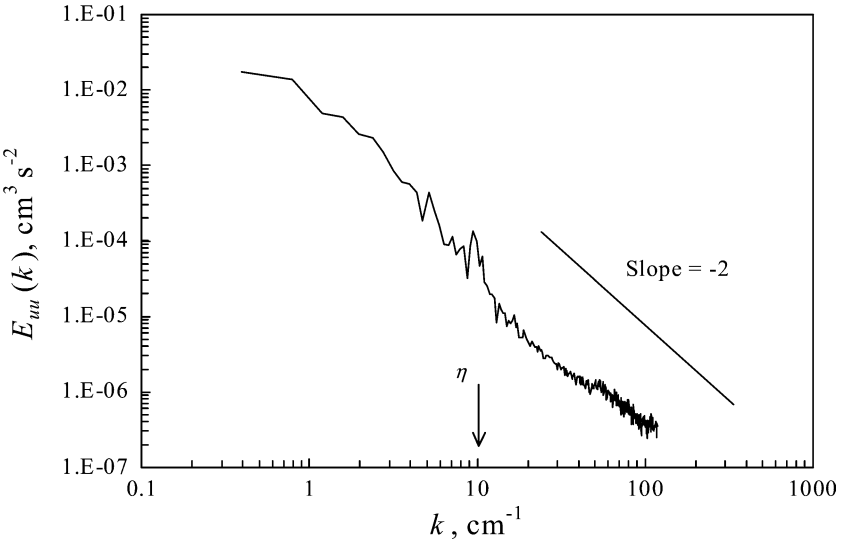

Fig. 4 A sample velocity spectrum from the current data ($Nt = 4.3$, St = 0.2). Both axes are dimensional and use logarithmic scaling. The location of the Kolmogorov scale η is indicated in the figure with an *arrow*. A line with a slope of -2 is included to show that curve decays at a rate slower than k^{-2} for the largest wavenumbers; convergence of the integral of $k^2 E_{uu}(k)$ is therefore not possible

$(du/dx)^2$ have a very large number of near-zero values, as is the case for the derivative of any random Gaussian variable; in contrast, the PDF of the true dissipation rate shows the probability of observing a zero value is zero (Tsinober 1993).

Definitions for the dissipation rate that rely on small-scale velocity derivatives can be used without the direct computation of velocity derivatives by computing the area under the dissipation spectra using the definition:

$$\int_0^\infty k^2 E_{uu}(k)\mathrm{d}k = \left(\frac{\partial u}{\partial x}\right)^2. \tag{4}$$

This definition has been used in several studies instead of directly computing the mean square velocity derivatives. For a specific example, Rohr et al. (1988) evaluated $k^2 \underline{E_{uu}(k)}$ and $k^2 E_{ww}(k)$ to estimate $\overline{(\partial u/\partial x)^2}$ and $\overline{(\partial w/\partial x)^2}$, then used Eq. 3 to estimate the dissipation rate. These spectral estimates must often be extrapolated to close the integral (Zhou and Antonia 2000), as the variance spectra may not decay faster than k^{-2}, and so the integral of Eq. 4 may not converge.

A velocity spectrum, E_{uu}, for the longitudinal velocity, u, is presented as Fig. 4 for data of density stratified turbulence (Nt = 4.3, St = 0.2). Indicated on the abscissa is the Kolmogorov length scale, η, for the time series (see Table 1 for values). Note that for wavenumbers in the vicinity of η spectral slopes decay as k^{-3}. For wavenumbers greater than η spectral slopes are approximately $-5/3$. A line with a slope of -2 is included: it is evident that on average the spectral slopes decays at a rate ($\sim -5/3$) slower than k^{-2} for the largest wavenumbers: thus convergence of the integral of $k^2 E_{uu}(k)$ is therefore not possible.

Data for the evolution of velocity variances of u, w are not shown for brevity. We note instead that the data for the decay of shear-free grid-generated turbulence follows the well-known empirical power law

$$\left(\frac{u_i'}{U}\right)^2 = A_i\left(\frac{x}{M} - C\right)^{-N} \tag{5}$$

where A_i, C and N are constants. The subscripts denote the longitudinal ($u_1 = u$) and vertical ($u_2 = w$) velocity components. The values of the constants $A_1 = 0.035$, $A_2 = 0.027$, $C = 3$ and $N = 1.1$ are in good agreement with previous studies (Comte-Bellot and Corrsin 1966). Substitution of these values in Eq. 5 facilitates evaluation of details of the velocity field (e.g., anisotropy ratio w/u). The slope of the best-fit line can be used to estimate a dissipation rate ε. Specifically, if $q^2 = 3u'^2$ then

$$U\frac{\mathrm{d}\frac{1}{2}\overline{q}^2}{\mathrm{d}x} = -\varepsilon \tag{6}$$

Then Eq. 6 can be written as

$$\varepsilon = -\frac{3}{2}\frac{\mathrm{d}}{\mathrm{d}t}(u'^2) = -\frac{3}{2}\overline{U}\frac{\mathrm{d}}{\mathrm{d}x}(u'^2) \tag{7}$$

where Taylor's Hypothesis has been used to change between the derivative forms. By simplifying the derivative with respect to x and substituting Eq. 5 for decaying grid generated turbulence into Eq. 7, one arrives at:

Table 1 A summary of statistics relating to the four specific time series discussed as examples

	Grid turbulence	Strongly sheared	Strongly stratified	Shear and stratification
Nt	0.3	0.5	4.3	4.7
St	0.4	4.3	0.2	5.1
Re_λ	24	29	13	33
$Re_{\lambda\rho}$	29	18	2	17
η (cm)	0.03	0.05	0.12	0.04
χ (g^2/cm^6/s)	4.0×10^{-11}	4.0×10^{-11}	2.8×10^{-10}	2.6×10^{-9}
ε (cm^2/s^3)	0.79	0.21	4.1×10^{-3}	0.27

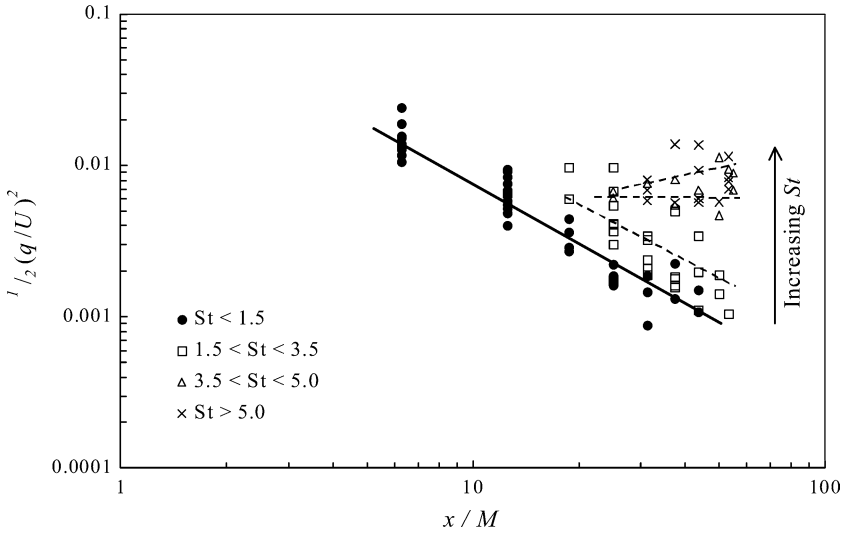

Fig. 5 Evolution of the dimensionless turbulent kinetic energy, $1/2(q/U)^2$, with dimensionless downstream distance, x/M, for four ranges of St. Included is a *solid line* with a slope of −1.1 for comparison with Eq. 5. The *dashed lines* show trends of increasing values of turbulent kinetic energy for increasing values of St

$$\varepsilon = \frac{3}{2} N A_1 \frac{\overline{U}^3}{M} \left(\frac{x}{M} - C \right)^{-N-1} \tag{8}$$

The balance method relies on the assumption that the decay of turbulent kinetic energy is due entirely to dissipation. If the rate of change of kinetic energy can be estimated downstream from a turbulence-generating grid (for example, using the empirical power law of Batchelor and Townsend 1948; Comte-Bellot and Corrsin 1966), and there are no sources or other sinks of kinetic energy in the flow, then the rate of dissipation can be estimated accurately. For studies investigating the relatively simple flow field of decaying grid-generated turbulence, this balance method has been used with success (e.g., Ma and Warhaft 1986; Jayesh and Warhaft 1994).

Evolution of turbulent kinetic energy (and velocity variances) for sheared flows are non-monotonic; this flow is more complex than that of decaying grid-generated turbulence and Eqs. 5, 6, 7 and 8 do not apply. The effects of shear are evident in Fig. 5. Values of non-dimensional turbulent kinetic energy $1/2(q/U)^2$ increase with increasing values of shear strain St. Indeed for the largest values of St, rather than a decay of $1/2(q/U)^2$ with distance x/M, values of $1/2(q/U)^2$ increase with distance x/M. For sheared turbulence, the decay rate of turbulent kinetic energy may be zero for intermediate values of St, $3.5 < St < 5$. For larger shear ($St > 5$) the decay rate is positive, i.e., that $\mathrm{d}/\mathrm{d}x(q^2/2)$ is positive. Therefore the balance method of evaluation that is represented by Eq. 6 cannot be utilized. Rather, for sheared flows Eq. 2 is used to estimate ε.

3.2 Correction method

Dissipation rates are required to compute numerous lengthscales and to scale several quantities. That there are a number of techniques used to estimate the dissipation rate of energy reflects that its accurate measurement is not a trivial matter. For the current experimental setup, a limit on the resolution of the velocity probe exists near the Kolmogorov scales of the flow. As discussed, the computation of the square of the longitudinal velocity derivative $\overline{(\mathrm{d}u/\mathrm{d}x)^2}$ shows significant variation for small values of Δx used in the computation. Not until a Δt of three data points (or 0.015 s) is used do the mean square values stabilize. Thus, one could obtain several different values of the dissipation rate ε varying up to a factor of ten by varying only this computational artifact. Computing the dissipation spectra $k^2 E_{uu}(k)$ was attempted. Initially, it was confirmed for numerous data points that the energy spectra $E_{uu}(k)$ (shown in Fig. 4) was correctly computed by comparing the integral $\int_0^\infty E_{uu}(k)\mathrm{d}k$ to the variance $\overline{u^2}$. Comparison between the integral computation (the area under the curve in Fig. 4) and the statistical measurement of the variance of $u(t)$ results in values that differ by only a fraction of a percent. However, computing the area under the dissipation spectra by evaluating $\int_0^\infty k^2 E_{uu}(k)\mathrm{d}k$ is less satisfactory. A plot of the construction of $k^2 E_{uu}(k)$ yields a horizontal line for large wavenumbers. The integral does not converge since for high wavenumbers where $E_{uu}(k) \sim k^{-2}$. Further, this area estimate does not equal $\overline{(\mathrm{d}u/\mathrm{d}x)^2}$ using any value of Δx.

An attempt was made to correct the energy spectra slope at high wavenumbers by extrapolating a steeper decay in the manner of Zhou and Antonia (2000). Convergence of the integral could be forced in this manner, but there was continued disagreement between the two methods. Specifically, $\overline{(\mathrm{d}u/\mathrm{d}x)^2}$ was being underestimated for a large portion of the data set in comparison with results for the value of the dissipation rate using Eq. 7. Forcing convergence of the dissipation spectra integral by manually increasing the decay rate of the line shown in Fig. 4 only produced smaller estimated values for $\overline{(\mathrm{d}u/\mathrm{d}x)^2}$. This correction results in values even farther away from those predicted using Eq. 7.

Corrections such as inclusion of, or relying solely on, the transverse velocity component (e.g., Eq. 3) also did not aid in increasing the estimate for the dissipation rate, as shown in Fig. 2.

This illustrates the dilemma that any of these methods used to estimate $\overline{(\mathrm{d}u/\mathrm{d}x)^2}$ results in values of the dissipation rate ε too low for a majority of the data. A solution to the problem would be to find an independent estimator for the dissipation rate or $\overline{(\mathrm{d}u/\mathrm{d}x)^2}$ that is independent of scales near the under-resolved Kolmogorov scales. For the case of stationary, homogeneous, isotropic turbulence, the dissipation rate appears in an intermediate equation in Kolmogorov's (1941a) search for universality. This expression was suggested to be valid for scales in the inertial range:

$$D_{\mathrm{uu}}(r) \sim C(\varepsilon r)^{2/3} \tag{9}$$

and states that the second-order velocity structure function (a function of separation distance r) scales as the product of the separation distance and average dissipation rate, each to the two-thirds power. In a subsequent paper, Kolmogorov (1941b), use is made of the Von Kármán and Howarth (1938) equation; which relates the derivative of the second-order longitudinal velocity structure function to the third-order structure function as:

$$D_{\mathrm{uuu}}(r) - 6\nu\frac{\mathrm{d}}{\mathrm{d}r}[D_{\mathrm{uu}}(r)] = -\frac{4}{5}\varepsilon r. \tag{10}$$

The validity of Eq. 10 has been established experimentally by, for example, Antonia et al. (1983) and Shah and Antonia (1986). This is an important equation in light of the current discussion. Both the second- and third-order structure functions are computed, though minor resolution challenges arise when the separation distances are near the Kolmogorov scales, $r \approx \eta$. However, the equation is valid over the inertial range scales, which the velocity probe can resolve fully. The scales of the inertial range vary with each time series of the current experiment: a typical range is $10 < r/\eta < 100$. This suggests that if experimental measurements can resolve approximately ten times the Kolmogorov scale, Eq. 10 can provide an estimate for the value of the dissipation rate by evaluating the left-hand side of Eq. 10. An initial estimate of $\overline{(\mathrm{d}u/\mathrm{d}x)^2}$ is required to make the correction, however. As the mean square gradient is based on $\Delta x \approx 2\eta$, minimum resolution finer than 10η is still required.

The proposed correction method includes the computation of $\overline{(\mathrm{d}u/\mathrm{d}x)^2}$ for all the data. From this mean square derivative, initial estimates for the Taylor microscale, λ, and the turbulent Reynolds number Re_λ are computed using the definitions:

$$\lambda^2 = u'^2/\overline{(\mathrm{d}u/\mathrm{d}x)^2} = 15\nu u'^2/\varepsilon, \tag{11}$$

$$\mathrm{Re}_\lambda = \frac{u'\lambda}{\nu}. \tag{12}$$

Second- and third-order structure functions are computed as well as the derivative of $D_{\mathrm{uu}}(r)$ with respect to r. These curves are then utilized in conjunction with Eq. 10 to obtain an estimate for the dissipation rate ε. Using the isotropic definition for the dissipation rate (Eq. 2) a new value for $\overline{(\mathrm{d}u/\mathrm{d}x)^2}$ for many data points are obtained. The computation of the mean square derivative is relatively easy during the course of data analysis; however, the graphical correction method must be performed manually on each data set. Thus, one would like to discern a general trend of the correction in terms of some easily computed quantity. If the trend is known, then this computation can then be performed, and the correction can be readily applied. Additionally, the quantification of the correction factor is important for future verification of this method in other flows. Therefore, a correction factor f_ε is defined as:

$$f_\varepsilon = \frac{\overline{(\mathrm{d}u/\mathrm{d}x)^2}_{\mathrm{new}}}{\overline{(\mathrm{d}u/\mathrm{d}x)^2}_{\mathrm{old}}}. \tag{13}$$

In a search for a variable to relate this factor to, it is reasonable that f_ε should depend on the initial estimate of the mean square derivative, and it was determined that including the rms velocity is optimal in collapsing the data. Recall that the need for dissipation rate corrections arises from inadequate probe resolution. Typically the spatial resolution of (hot-film) velocity probes is of the order of the Kolmogorov length scale; the value of the Kolmogorov length scale decreases with increasing values of Reynolds number. Thus dissipation rates are increasingly underestimated with increasing Reynolds number. Therefore an empirical correction function based on a Reynolds number is proposed. The best results are obtained when f_ε is plotted against the original estimate of Re_λ, yielding:

$$f_\varepsilon = \frac{\mathrm{Re}_\lambda}{16}. \tag{14}$$

The value of this adjustment factor f_ε varies from 0.5 to about 8 in the current experiment. New values for $\overline{(\mathrm{d}u/\mathrm{d}x)^2}$ are then computed, along with all quantities that are derived from it (e.g., λ and ε).

A consideration is that for low Reynolds numbers the limited scale separation between the large and small scales limits the validity of Eq. 10. Therefore, the effects of the large scales on the dynamics of the dissipative scales must be taken into account by considering a source term. Equation 10 can be modified to include a source term, S_u, on the left-hand side of Eq. 10.

$$D_{\mathrm{uuu}}(r) - 6\nu\frac{\mathrm{d}}{\mathrm{d}r}[D_{\mathrm{uu}}(r)] + S_u = -\frac{4}{5}\varepsilon r. \tag{15}$$

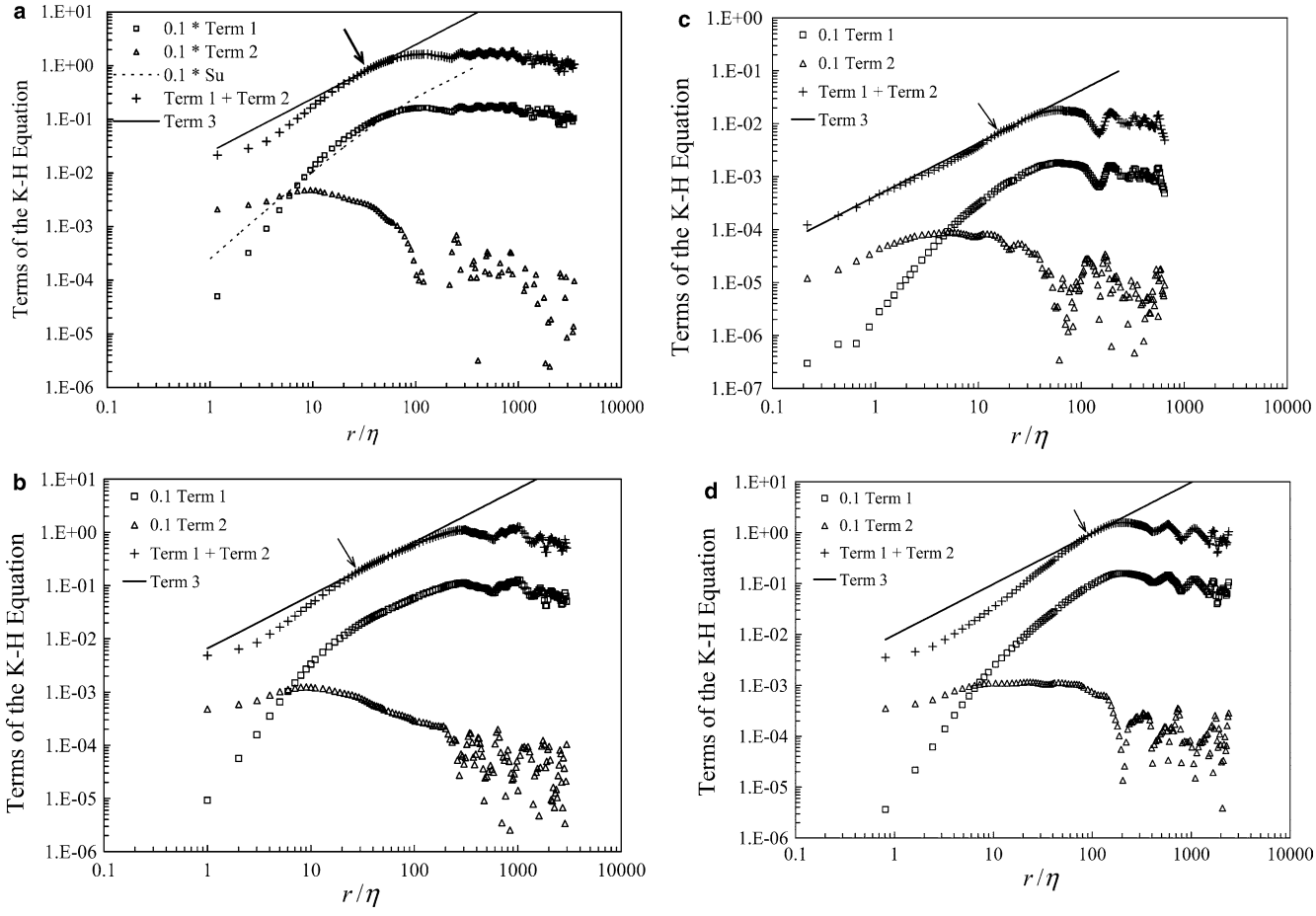

Fig. 6 Graphical representation of an estimate of the turbulent kinetic energy dissipation rate ε. Plotted on the ordinate are the three terms of Eq. 10 (the Karman–Howarth equation): the abscissa is non-dimensionalized by the Kolmogorov length scale η. Term 1 is the third-order velocity structure function; Term 2 is 6ν times the rate of change of the second-order structure function with separation distance r. To ease interpretation, both of these curves are shifted down by one decade. The sum of these two terms is indicated by the + symbol. Term 3 is $\frac{4}{5}\epsilon r$ where ε has been adjusted to bring the line tangent to the left-hand side of Eq. 10. The data in **a** are for a flow with Nt = 0.3, St = 0.4, which represents decaying grid turbulence. The *thin dashed line* in **a** is the estimated magnitude of the source term S_u (also shifted down by one decade), of Eq. 16. For **b** Nt = 0.5, St = 4.3 and reflects a strongly sheared flow. **c** is a strongly stratified flow for which Nt = 4.3, St = 0.2. Finally, for **d** Nt = 4.7, $St = 5.1$ so that the flow is influenced by both stratification and shear. An *arrow* indicates the point of tangency in the inertial subrange

For the case of stationary, isotropic homogeneous turbulence the form of the source term S_u has been determined by Danaila et al. (1999). The form of the source term depends on the characteristics of the large scales of the turbulence field: large scale characteristics depend on the details of turbulence production or attenuation mechanisms such as velocity shear or density stratification, respectively. For the case of decaying grid-generated turbulence Danaila et al. obtained

$$S_u = -3\frac{U}{r^4}\int_0^r y^4 \frac{\partial}{\partial x}(\Delta u_1)^2 \mathrm{d}y. \qquad (16)$$

Data are presented in Fig. 6, in which are shown the three individual terms of Eq. 10. For clarity the individual terms of the left-hand side have been shifted down by a decade. Note that for the flow fields of Fig. 6 we evaluate the balance of Eq. 10 rather than Eq. 15 because the form of the source term is only known for the flow-field of decaying grid-generated turbulence. Therefore, a method is developed for estimating dissipation rates which does not require measurements of S_u.

For the present data of decaying grid-generated turbulence presented in Fig. 6a, it is possible to estimate the magnitude of the source term by evaluating the integral of Eq. 16. This has been done, and this estimate is also shown in Fig. 6a. For small separation distances $1 < r/\eta < 5$ the major contribution is from the viscous term $6\nu\frac{\mathrm{d}}{\mathrm{d}r}[D_{\mathrm{uu}}(r)]$. Note that the contribution from the viscous term diminishes towards zero for large separation distances $r/\eta > 50$. The turbulent transport term $D_{\mathrm{uuu}}(r)$ is the largest term for $10 < r/\eta < 200$. The magnitude of the source term is comparable in magnitude to the other terms for $r/\eta < 200$. For $r/\eta > 200$, the source term is the largest contributor.

The slopes of the turbulent transport and viscous terms (terms 1 and 2 in Eq. 10) require comment. For large values of r, term 1 should vary as r; for small values of r, term 2 should vary as r. This is corroborated by the data of Fig. 6a. For $r\eta \sim O(10)$, the slope of term 1 is approximately $+1$. Due to finite probe resolution near Kolmogorov scales $r = \eta$ the slope of term 2 only asymptotes towards an r^{+1} dependence. This is also true of previous studies. For example, a similar asymptotic approach of term 2 to a, r^{+1} dependence is evident in the data of Figs. 3 and 4 of Danaila et al. (1999).

The term $4/5\ \varepsilon r$ should equal the sum of all the other terms in Eq. 10. Note that the sum of the values of structure function and viscous terms in Eq. 10 is approximately equal to $4/5\ \varepsilon\ r$ for values of r/η up to 30. For values of r/η larger than 30, the contribution of the source term becomes significant. Thus, the location of the point of tangency is $\sim 30\eta$. Note that at the point of tangency the ratio of the turbulent transport term to the source term is 1.6; the ratio of the source term to $(4/5\ \varepsilon\ r)$ is approximately 0.6; and the ratio of the viscous term to $(4/5\ \varepsilon\ r)$ is about 0.04. Our values are in good agreement with the data available for decaying grid-generated turbulence. For example, our maximum value for the normalized third-order structure function is 0.62: this is in accord with the value of 0.43 obtained by Zhou and Antonia (2000) in their wind-tunnel experiments, and 0.49 in DNS simulations by Orlandi and Antonia (2002). Comparison of data for the point of tangency ($\sim 30\ r/\eta$) of the third-order structure function to the line $(4/5\ \varepsilon r)$ are also in accord with the point of tangency occurring at $r/\eta \sim 30$, 20, 20 for the present data, Orlandi and Antonia (2002) and Danaila et al. (1999), respectively.

The locations of the point of tangency for the case of decaying grid-generated turbulence for the present low Reynolds numbers experiments (see Table 1) together with the data for the large Reynolds number results of Mydlarski and Warhaft (1996) for which R_λ where 99 and 448 are shown in Fig. 7. Experiments with increasing values of R_λ possess larger ranges of the inertial subrange. Thus, for the data of Mydlarski and Warhaft, the source correction term, S_u, becomes significant at larger values of r/η due to the larger values of R_λ of their data; therefore, the point of tangency also occurs at larger values of r/η. The best fit line for r/η values of the location of the point of tangency varies as $R_\lambda{}^{+1}$. This arises because r is an integral scale measure, and it is known that integral scales l are related to the Taylor microscale λ as $l/\lambda \sim R_\lambda{}^{+1}$ (Tennekes and Lumley 1982).

Data of experiments with low values of Re_λ (for the current experiments, $Re_\lambda < 50$) will not obtain agreement over large ranges (i.e., a decade in r/η). However, a large range of r/η is not required for the proposed technique to work. The estimate of the dissipation rate is obtained by plotting the terms of Eq. 10 against r/η on a log–log scale. The sum of the structure function and the viscous term on the left-hand side, $\left(D_{uuu}(r) - 6\nu\frac{d}{dr}[D_{uu}(r)]\right)$, increases with increasing values of r/η. The point of tangency dictates the value of ε (for Fig. 6a the point of tangency occurs at $r/\eta = 30$). The value of the right-hand side $(4/5\ \varepsilon r)$ is chosen such that it is equal to the value of the sum of the left-hand side of Eq. 10 at the point of tangency.

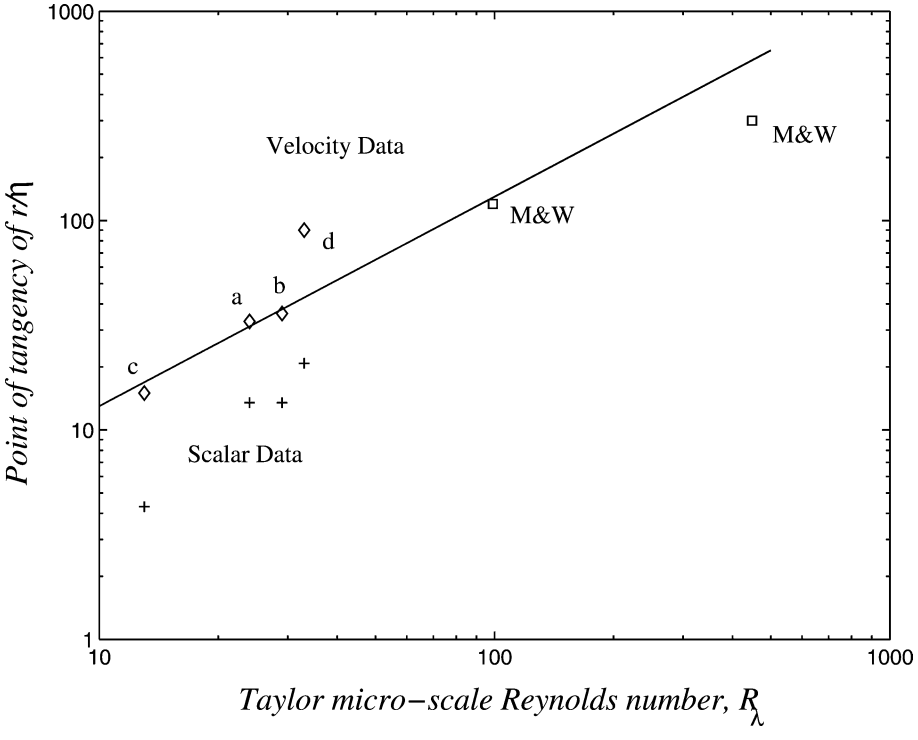

Fig. 7 Dependence of the location of the point of tangency of the sum of the third-order velocity structure function, $D_{uuu}(r)$, and the viscous term, $6\nu\frac{d}{dr}[D_{uu}(r)]$, to the line $(4/5\ \varepsilon r)$. Velocity data presented in this study are shown as **a**, **b**, **c**, and **d**, that represent decaying grid generated, sheared, density stratified, and sheared and density stratified turbulence, respectively. Also shown are the data of Mydlarski and Warhaft (1996) as analyzed by Danaila et al. (1999). The best-fit line to velocity data has a slope of $+1$. Locations of points of tangency of the scalar mixed moment data $(+)$ for (**a**), (**b**), (**c**), (**d**) are also shown. (Note that scalar data are for $Sc = 700$.)

The data comprising Fig. 6a are for time series for which the turbulence-generating grid dominates the dynamics (i.e., decaying grid-generated turbulence): neither Nt nor St is large (Nt = 0.3, St = 0.4). Figure 6b shows data obtained for shear-dominated turbulence (Nt = 0.5, St = 4.3). Presented in Fig. 6c are data from a density stratified region where the buoyancy strain dominates (Nt = 4.3, St = 0.2); and in Fig. 6d, data are from a region with both strong shear and strong density stratification (Nt = 4.7, St = 5.1). For reference, statistics from these four representative data points are tabulated in Table 1. Notice that in each of these figures, the curvature of the line representing the sum of the terms on the left-hand side is such that it becomes tangent to the line (4/5 ε r) in the inertial range. Examination of velocity spectra shows that the inertial range occurs approximately between 10 and 100 $r\eta$. Analysis of the data for sheared turbulence (Fig. 6b) shows that the turbulent transport and viscous terms are approximately parallel to 4/5 εr up to 130 r/η. This compares with 70 r/η for the decaying grid-generated turbulence data of Fig. 6a. This difference is consistent with a larger inertial sub-range arising from gradient production of turbulence by velocity shear. For the data of turbulence influenced by density stratification (Fig. 6c) the sum of the turbulent transport and viscous terms is approximately parallel to 4/5ε r up to 50 r/η. This is in accord with the expected attenuation of turbulence intensities by stable density stratification. The location of the point of tangency is at 15 r/η as compared to 30 r/η for the data of decaying grid generated and sheared turbulence. Note that the magnitudes of both the ordinate and abscissa are smaller for the data of density stratified turbulence. Ordinate values decrease due to smaller levels of turbulence energies: abscissa values are smaller as the values of the Kolmogorov scale $\eta = (\nu^3/\varepsilon)^{1/4}$ are larger (see Table 1) than for decaying grid generated and sheared turbulence cases. For the complex case of sheared and density stratified turbulence the data of Fig. 6d reveals a point of tangency at approximately 90 r/η. The four flow conditions of Fig. 6a, b, c, d represent widely varying dynamics. To emphasize the point: it is evident that the Karman–Howarth equality (Eq. 10) which relates second- and third-order structure functions to dissipation rates is valid for both unstrained turbulence (decaying grid-generated turbulence), and strained turbulence at least up to the magnitudes of strains of the current experiments ($Nt\sim$ 10, $St\sim$ 10). This flexible utility suggests that the proposed technique for estimating dissipation rates will be widely useful in assessing dissipation rates of turbulent kinetic energy. (There are few other data sets of strained turbulence to compare. The present results are in accord with the experiments of Moisy et al. (1999) who determined, for turbulence generated by discs rotating in opposite directions in a cylinder, that the second and third-order structure functions were accurately related by the Karman–Howarth equation with a forcing term.)

4 Scalar dissipation

4.1 Definitions

The scalar dissipation rate concerns the destruction of the scalar variance. For a passive scalar with Sc≈1, the characteristics of the scalar field may be similar to the velocity field. The smallest scale required to resolve the turbulent velocity and scalar fields in such a flow (Sc = 1) is approximately the Kolmogorov scale, η. However, the current salt-stratified flow has a Schmidt number Sc≈700; therefore, the Batchelor scale $\eta_B = \eta Sc^{-1/2}$, rather than the Kolmogorov scale, is the smallest scale of concern. This fact suggests that dissipation, which occurs at very small scales, may not be as well resolved for the scalar field as compared to the velocity field.

The definition of the scalar dissipation rate is:

$$\chi = \varepsilon_\theta = 2\alpha\left(\overline{(\partial\theta/\partial x)^2} + \overline{(\partial\theta/\partial y)^2} + \overline{(\partial\theta/\partial z)^2}\right), \qquad (17)$$

where θ is the fluctuating temperature, and α is the scalar diffusivity. In many studies, the notation for scalar dissipation rate is often ε_θ for the thermal dissipation rate, or ε_ρ when the scalar is salt; however, the more concise notation of χ is used here. As for the kinetic energy dissipation rate, complete resolution of scalar dissipation requires the measurement of several gradients. Specifically, more than one set of probes would be required to resolve the vertical and transverse gradients, even if the longitudinal derivative is obtained using Taylor's hypothesis (e.g., utilizing the four-wire probe of Sreenivasan et al. 1977). Even though temperature and salinity are scalars, their dissipation rates can still be affected by anisotropy, as has been discussed by Mydlarski and Warhaft 1998; Nash and Moum 2002. For example, for strongly density-stratified turbulence, the anisotropy of large and small scale density gradients may be significant. The degree of isotropy is found to be important occasionally, although errors induced by measurement techniques can outweigh this inaccuracy (Thoroddsen and Van Atta 1996). Thus, in practice, isotropy of small scales is usually assumed. The scalar dissipation rate can therefore be estimated by computing only the longitudinal derivative: assuming that all three gradients make a similar contribution to dissipation of the scalar (Gibson and Masiello 1972):

$$\chi = 6\alpha\overline{(\partial\theta/\partial x)^2} = 6D\overline{(\partial\rho/\partial x)^2}. \qquad (18)$$

Equation 18 introduces the notation used for the current salt-stratified water experiments. The density fluctuation ρ has replaced the temperature fluctuation θ, and D, the diffusivity of salt in water, has replaced thermal diffusivity α.

Similar to the calculation for the dissipation rate of turbulent kinetic energy, the scalar dissipation rate can be determined through several avenues. For example, the mean square scalar derivative (and therefore χ via

Eq. 18) may be computed from the scalar dissipation spectrum:

$$\int_0^\infty k^2 E_{\rho\rho}(k)\mathrm{d}k = \overline{(\partial\rho/\partial x)^2}. \tag{19}$$

This scalar spectrum must often be extrapolated to close the integral (Zhou and Antonia 2000). Alternatively, the scalar dissipation rate can be estimated by a balance method through the computation of the other terms in the scalar variance evolution equation (see Appendix):

$$U\frac{\partial\rho^2}{\partial x} = -2\overline{\rho w}\frac{\partial\overline{\rho}}{\partial z} - \chi \tag{20}$$

This method has been used in experimental studies of shear-free turbulence for both salt-stratified water (Itsweire et al. 1986) and heat-stratified air (Thoroddsen and Van Atta 1996). Note that the buoyancy term in Eq. 20 may be either a source or a sink. Thus, the rate of change of the scalar variance may be difficult to estimate via Eq. 20 for density stratified flows (i.e.,) $\partial\bar{\rho}/\partial z \neq 0$. For example, the mean vertical buoyancy flux $\overline{\rho w}$ can change sign in shear-free, stratified grid-generated turbulence (Itsweire et al. 1986; Huq and Britter 1995b). When this sign change occurs, the first term on the right-hand side of Eq. 20 becomes a sink, thus affecting the downstream evolution of scalar variance. The difficulty in using Eq. 20 for such complex flow has been noted previously. For example, Yoon and Warhaft (1990) used the spectral method to estimate the scalar dissipation rate of heat in air for their experiments: χ could not be estimated from the balance equation because the term $\mathrm{d}(\rho^2)/\mathrm{d}x$ changed sign.

4.2 Correction of the scalar dissipation rate estimate

Magnitudes of the correction for the scalar dissipation rate, χ, are greater for the current experimental configuration than the correction for the energy dissipation rate ε. For the latter case, the limiting resolution is that of the Kolmogorov scale. In the former case, with salt in water (where $S_u = 700$), the ratio of the Batchelor to the Kolmogorov lengthscale is 26. Therefore, almost 30× the spatial resolution is required to resolve the scalar dissipation rate fully using any of the methods discussed previously. This resolution is difficult to attain. The consensus of theoretical scalar spectra (Batchelor 1959) suggests that there is considerable spectral density beyond the Kolmogorov wavenumber, and that $E_{\rho\rho}(k) \sim (k\eta)^{-1}$ for $k > \eta$. The slow decay $(k\eta)^{-1}$ makes the determination of scalar dissipation rate difficult as closure of the integral of $k^2 E_{\rho\rho}(k)$ cannot be obtained until the scalar spectrum decays at a rate faster than -2.

The proposed technique for correcting the scalar dissipation rate parallels the previously presented technique for correction of the kinetic energy dissipation rate. The theoretical expression of the scalar-mixed moment structure function determined by Yaglom (1949) produces a similar form as the Karman–Howarth equation (10).

$$D_{u\rho\rho}(r) - 2\kappa\frac{\partial}{\partial r}D_{\rho\rho}(r) = -\frac{4}{3}\chi r. \tag{21}$$

This equation predicts that for turbulent passive scalar fields the scalar-mixed moment $D_{u\rho\rho}$ and the second-order scalar term $\kappa\frac{\partial}{\partial r}D_{\rho\rho}(r)$ are balanced by scalar dissipation term $4/3\ \chi\ r$ in the inertial sub-range. Equation 21 has been verified by measurements (see Monin and Yaglom 1971; Antonia et al. 1983). For flows with large Reynolds and Peclet ($=ul/\kappa$) numbers, the Yaglom equation (Eq. 21) simplifies to the two term balance of Eq. 22 (Warhaft 2000):

$$D_{u\rho\rho}(r) = \frac{4}{3}\chi r. \tag{22}$$

This predicts that the scalar-mixed moment structure function depends only on a constant coefficient, the separation distance r, and the scalar dissipation rate. The right-hand side is the product of a constant, the scalar dissipation rate χ, and the separation distance r. The left-hand side is the definition of the scalar-mixed moment structure function. Its construction, the product of a first-order longitudinal velocity increment and a second-order scalar increment, is similar to the turbulent transport term $u\rho^2$ in the scalar variance evolution equation (e.g., see Townsend 1980). A similar type of construction, the mixed derivative skewness, has previously been presented for passive scalar data (Wyngaard 1971; Antonia and Chambers 1980). The range of validity of this equation is the inertial range of scales.

The left-hand side of Eq. 22 is easily computed from measured velocity and scalar time series. The only unknown on the right-hand side is the scalar dissipation rate χ. Similar to the previous correction method used to determine ε, the value of scalar dissipation rate can be set such that the right-hand side of Eq. 22 is equal to the mixed moment structure function.

As for the turbulent velocity field, the consequence of low Reynolds number flows is the non-stationarity of statistical quantities due to the interaction between the large (integral) and smaller scales. Danaila et al. (1999) have shown that this is accounted for by a source term S_ρ, so yielding:

$$D_{u\rho\rho}(r) - 2\kappa\frac{\partial}{\partial r}D_{\rho\rho}(r) + S_\rho = -\frac{4}{3}\chi r. \tag{23}$$

Only for the case of decaying grid-generated turbulence has the form of the source term been evaluated (Danaila et al. 1999). The proposed correction method for the scalar field parallels the correction method for the velocity field, and we neglect the contribution of the source term. Thus, values of χ are estimated, as described, without measurements of S_ρ.

Determination of the scalar dissipation rate using Eq. 22 has been undertaken for the various flow fields (decaying grid-generated turbulence; sheared turbulence; density stratified turbulence; and sheared density stratified turbulence). Derived values of χ were used in conjunction with Eq. 18 to retrieve a value for the mean square longitudinal derivative of the scalar, $\overline{(\mathrm{d}\rho/\mathrm{d}x)^2}$. The values of this quantity were compared to the original estimate, computed in the same manner as $\overline{(\mathrm{d}u/\mathrm{d}x)^2}$ discussed previously in Sect. 2.3 where the derivative was computed using a separation distance of three points ($3\Delta t \approx 2\eta$). The correction factor for this scalar derivative should be a function of a scalar turbulent Reynolds number. Thus, using the original estimate for $\overline{(\mathrm{d}\rho/\mathrm{d}x)^2}$, a scalar Taylor microscale is computed:

$$\lambda_\rho^2 = \rho'^2/\overline{(\mathrm{d}\rho/\mathrm{d}x)^2}. \tag{24}$$

This equation is similar to the definition for the Taylor lengthscale based on the velocity field (Eq. 11), but the rms density fluctuations ρ' have replaced the longitudinal velocity u'. A scalar turbulent Reynolds number can then be defined as:

$$\mathrm{Re}_{\lambda\rho} = \frac{u'\lambda_\rho}{\nu}. \tag{25}$$

Following the previous method for the kinetic energy dissipation rate, a correction factor f_χ can be defined:

$$f_\chi = \frac{\overline{(\mathrm{d}\rho/\mathrm{d}x)^2}_{\mathrm{new}}}{\overline{(\mathrm{d}\rho/\mathrm{d}x)^2}_{\mathrm{old}}}. \tag{26}$$

If the form of this correction factor (related to some easily measured quantity) is known, the manual graphical method need not be applied to every measured time series. After computing this factor for numerous time series, the correction factor was found to vary as a function of $\mathrm{Re}_{\lambda\rho}$:

$$f_\chi = 16\mathrm{Re}_{\lambda\rho}. \tag{27}$$

The above correction function was applied to the originally estimated $\overline{(\mathrm{d}\rho/\mathrm{d}x)^2}$, and subsequently used to compute the scalar dissipation rate. Magnitudes of the correction factors for the scalar dissipation rate for the current data range from about 30 to 750. Note that the value of the constant of the scalar correction function (Eq. 27) is much larger than the value of the constant of the kinetic energy dissipation rate function (Eq. 14), and thus the magnitudes of the corrections are also larger. This is to be expected for the large Schmidt number flow of the experiment where scalar dissipation occurs on Batchelor rather than Kolmogorov scales.

Examples for this correction method are provided graphically in Fig. 8a through Fig. 8d. The data are from the same data sets used for the kinetic energy dissipation rate examples and are tabulated in Table 1. The scalar-mixed moment structure function, the left-hand side of Eq. 22, is plotted on a log–log plot against the separation distance non-dimensionalized by the Batchelor scale η_β. The line representing the right-hand side of Eq. 22, with χ set such that it is tangent to the data, is also shown. The dissipation rate estimate is chosen such that it is tangent to the scalar mixed moment structure function in the scalar inertial range of each respective time series; this point is indicated by an arrow on each figure. In Fig. 8a (Nt = 0.3, St = 0.4), values of the scalar mixed moment structure function, $D_{u\rho\rho}$ (r), rise quickly at a slope of approximately $(r/\eta_B)^2$ for values of $r/\eta_B < 250$. The right-hand side of Eq. 22, 4/3 χ r, is tangent to the curve of the scalar mixed moment structure function at $r/\eta_B \sim 338$. For $r\eta_B > 3{,}000$, the value of the scalar mixed moment structure function maintains approximately constant values for increasing values of r/η_B. The approximately constant value of the scalar structure function for $r/\eta_B > 3{,}000$ (or $r/\eta > 100$) is consistent with the production of scalar fluctuations due to turbulence interaction with the gradient of passive scalar (see Fig. 2) at large (integral) scales. Note that in the absence of a passive scalar gradient, values of the scalar mixed moment structure function, $D_{u\rho\rho}$ (r), decrease at integral scales (Danaila et al. 1999; Orlandi and Antonia 2002). The data for sheared turbulence velocity, with density stratification, and for the case with velocity shear and density stratification are presented in Fig. 8b, c, d, respectively. The evolution of the scalar mixed moment structure function with r/η_B for Fig. 8b, c, d are broadly similar to Fig. 8a.

A note is made on the location of the inertial range for the scalar signal. As Zhou and Antonia (2000) comment, the inertial ranges for the scalar and velocity fields (even for a passive scalar) are not required to be the same; differences between the dynamics of the velocity field and a passive scalar field were recognized earlier by Kraichnan (1968). The scalar signal may exhibit inertial range behavior for smaller separation distances than the velocity signal, and Tong and Warhaft (1994) make note of this shift to smaller scales. Jayesh et al. (1994) point out that a proper scaling region may not be expected to exist in such low-Re_λ flows as a true cascade through the inertial range may not occur; but if a scaling range does exist, it may appear first in the scalar signal, and then in the velocity signal. It should also be noted that the velocity data of Fig. 6a was non-dimensionalized by the Kolmogorov scale, $\eta = 0.03$ cm, while the scalar data of Fig. 8a has been non-dimensionalized by the Batchelor scale, $\eta_B = 0.0012$ cm. For the current experiment, the inertial range for the velocity signal varies by time series, but often occurs in the range $10 < r/\eta < 100$, and the tangential asymptote for the velocity dissipation rate correction is found at $r/\eta = \mathrm{O}(10)$; the four sample data sets shown in Fig. 6a, b, c, d have tangents located at $r/\eta = 33$, 36, 15, and 90, respectively. For the scalar signal, the inertial range again varies by time series, but the typical range is $100 < r/\eta_\beta < 1{,}500$, approximately

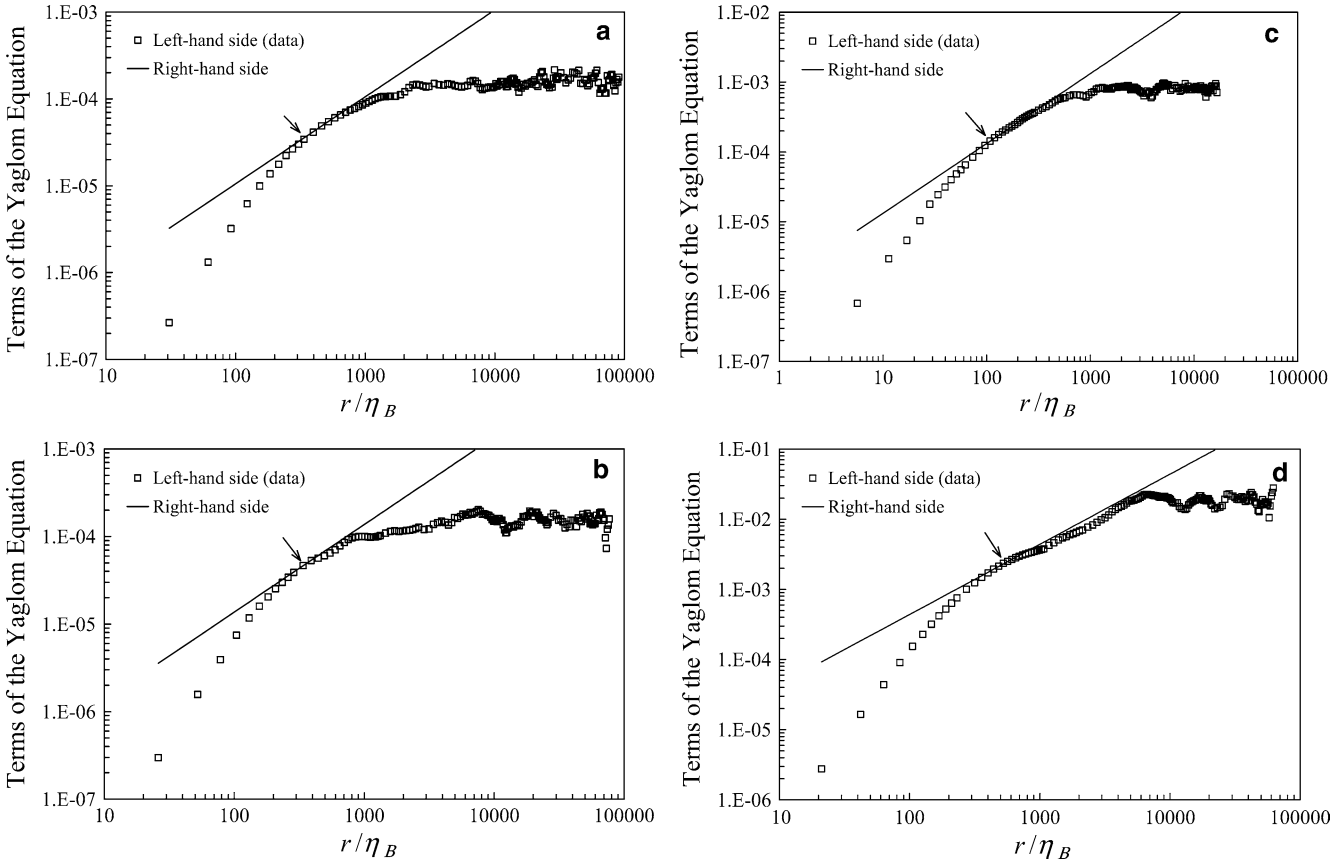

Fig. 8 An example of estimating the scalar dissipation rate χ. Plotted on the ordinate are the terms of the Yaglom equation (Eq. 22). Note that the abscissa has been non-dimensionalized by the Batchelor scale η_B. Shown on the ordinate are the left-hand side of Eq. 22, the scalar-mixed moment structure function ($D_{u\rho\ \rho}(r)$), and the right-hand side, $\frac{4}{3}\chi r$.The data in **a** are for a flow with Nt = 0.3, St = 0.4, which represents decaying grid turbulence. For **b**, Nt = 0.5, St = 4.3 and reflects a strongly sheared flow. **c** is a strongly stratified flow for which Nt = 4.3, St = 0.2. Finally, for **d** Nt = 4.7, St = 5.1 so that the flow is influenced by both stratification and shear. An *arrow* indicates the point of tangency

corresponding to $5 < r/\eta < 50$. The points of tangency for the scalar field are located at r/η_β = 338, 338, 107, 520 for the four representative cases shown in Fig. 8a, b, c, d: the location of the point of tangency increases with R_λ. Data of the points of tangency, for both velocity and scalar, are shown in Fig. 7. It is evident that the scalar signal attains tangency at smaller values of r/η. On average, tangency occurs at approximately one quarter of the value of r/η of the location of tangency of the velocity signal. Extrapolation of the data suggests that the scalar and velocity fields develop at similar scales for values of $R_\lambda \sim 10^3$.

The present data are for Sc = 700, and the point of tangency for the scalar mixed moment evolves as $r/\eta = f R_\lambda^M$ with $M = 1.5$ and $f = 0.1$. Comparison with the wind-tunnel data (Pr = 0.7) of Danaila et al. (1999) and the DNS results of Orlandi and Antonia (2002) suggests a weak dependence on Sc of the value of the constant f; this variation is well represented by $f = g\ (Sc^Q)$ with $Q = 0.1$ and $g = 0.05$. Thus the location of the point of tangency of the scalar mixed moment is given by $r/\eta = (0.05Sc^{0.1})\ R_\lambda^{1.5}$.

4.3 Comparison of estimation methods

It is possible to evaluate the effectiveness of the proposed correction method: for a given data point, the scalar variance is computed from the balance of terms in Eq. 20. Estimates are also computed from the original estimate of $\overline{(d\rho/dx)^2}$, the integration of the scalar spectra, and the correction factor defined by Eq. 27. The specific data point used for comparative purposes has values of the dimensionless shear and stratification, St = 0.2 and Nt = 4.3. Results are summarized in Table 2.

This particular point was chosen specifically to be shear free, and to be in a region where the scalar variance is decaying at a steady rate. Thus, Eq. 20 can be solved, and will be used to compare the other estimates. The solution of Eq. 20 results in a value of $\overline{(d\rho/dx)^2} = 9.21 \times 10^{-5} g^2/cm^8 (\chi = 7.89 \times 10^{-9} g/cm^6/s)$. The scalar variance wavenumber spectrum for this data point is plotted in Fig. 9. For values of wavenumbers corresponding to the Kolmogorov scale η, the scalar spectrum

Table 2 A summary of estimated values of the scalar dissipation rate using a variety of methods discussed in the text and a comparison to the most accurate estimate

Method	Estimated χ (g^2 cm^6/s)	Estimate/balance method estimate
Balance	7.89×10^{-9}	1
Area under spectra	4.43×10^{-11}	5.6×10^{-3}
Area under extrapolated spectra	7.93×10^{-11}	1.0×10^{-2}
Mean square derivative	2.60×10^{-11}	3.3×10^{-3}
Corrected mean square derivative	3.13×10^{-9}	0.40

evolves as k^{-1}. For wavenumbers corresponding to 2η the scalar spectrum evolves as k^{-2} till about $k\sim 50\text{cm}^{-1}$: for $k>50\text{cm}^{-1}$, the spectrum evolves as k^{-1} i.e., $E(k)$ decays at a rate slower than k^{-2}. The best estimate of the scalar dissipation rate would require resolution of this spectrum out to the Batchelor wavenumber, indicated by η_β. To obtain the scalar dissipation rate from such spectrum, integration is required in the form of Eq. 19. However, for wavenumbers greater than about 50 cm^{-1}, $E_{\rho\ \rho}(k)$ decays at a rate slower than k^{-2}. Therefore, the integral of $k^2\ E_{\rho\ \rho}(k)$ does not converge. For completeness, the area under the curve (out to $k\approx 115\ \text{cm}^{-1}$) was computed and resulted in $\overline{(\mathrm{d}\rho/\mathrm{d}x)^2} = 5.17\times10^{-7}\text{g}^2/\text{cm}^8$. (or $\chi=4.43\times10^{-11}$ $\text{g/cm}^6/\text{s}$). If the spectrum is estimated out to the Batchelor wavenumber by assuming that $E_{\rho\rho}(k)$ decays as k^{-4} for $k>65\ \text{cm}^{-1}$ and extrapolating the curve, the estimate for the area under the curve decreases to $\overline{(\mathrm{d}\rho/\mathrm{d}x)^2} = 4.93\times10^{-7}\text{g}^2/\text{cm}^8$. One could alternatively extrapolate the spectra as k^{-1} for $k>90$ (shown schematically in Fig. 8.1 of Townsend 1980, for example) until about the Batchelor scale, after which it would decrease sharply. This method of extrapolation produces an area estimate of $\overline{(\mathrm{d}\rho/\mathrm{d}x)^2} = 9.25\times10^{-7}\text{g}^2/\text{cm}^8$ ($\chi=7.93\times10^{-11}\text{g}^2/\text{cm}^6/\text{s}$).

The initial estimate for $\overline{(\mathrm{d}\rho/\mathrm{d}x)^2}$ using a separation distance of three points in the time series to compute the derivative results in an estimate of $\overline{(\mathrm{d}\rho/\mathrm{d}x)^2} = 3.03\times10^{-7}\text{g}^2/\text{cm}^7$ ($\chi=2.60\times10^{-11}\text{g}^2/\text{cm}^6/\text{s}$). Finally, the correction method proposed in this study (based on the scalar-mixed moment structure function outlined above) for this data point produces an estimate over 120 times larger; $\overline{(\mathrm{d}\rho/\mathrm{d}x)^2} = 3.65\times10^{-5}\text{g}^2/\text{cm}^8$ ($\chi=3.13\times10^{-9}\text{g}^2/\text{cm}^6/\text{s}$). This estimate is obtained using the three-point separation value for $\overline{(\mathrm{d}\rho/\mathrm{d}x)^2}$ and $\text{Re}_{\lambda\rho}=7.52$. Thus, it has been demonstrated that the proposed correction factor results in a scalar dissipation rate of the same order as the correct value. This demonstration establishes the utility of the proposed correction procedure based on Eq. 22. A scalar dissipation rate that had been underestimated by a factor of more than 100 is estimated to within a factor of 2. In light of the possible (unknown) errors in the evaluation of the terms in Eq. 22, the utility of the proposed method is clearly demonstrated. One may question if the leading constant of Eq. 27 should vary with Pr (or Sc). The present experiments are limited to flows for which Sc = 700, and thus we are unable to address the question of the dependence of the constant on Pr (or Sc).

5 Conclusion

The dissipation rates of the turbulent kinetic energy and of the scalar in the current flow fields are underestimated using standard measurement and evaluation techniques. The dissipation rate of kinetic energy is underestimated due to a lack of resolution. Measurements are resolved within a factor of two or three Kolmogorov scales rather than to the Kolmogorov scale, and values of correction factors for this dissipation rate are O(1). Estimates of the scalar dissipation rate are underestimated also because of inadequate resolution even though scalar scales are resolved down to the Kolmogorov scales. Resolution down to the Batchelor scale is required to determine scalar dissipation; for this high Schmidt number flow

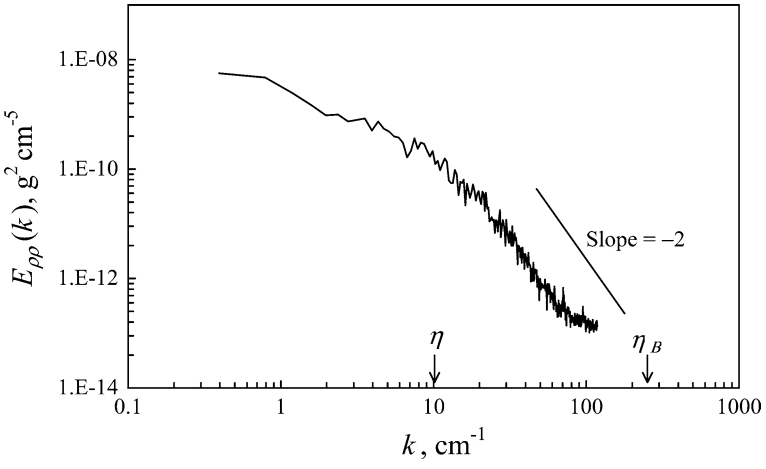

Fig. 9 A sample scalar wavenumber spectrum from the current data ($Nt=4.3$, $\text{St}=0.2$). Both axes are dimensional and have logarithmic scaling. The location of the Kolmogorov scale η and the Batchelor scale η_β are indicated on the figure with *arrows*. A line with a slope of −2 is included to show that the curve decays at a rate slower than k^{-2} for the largest wavenumbers ($k>50$); convergence of the integral of $k^2E_{\rho\ \rho}(k)$ is therefore not possible

(Sc = 700) the Batchelor scale is 30× smaller than the Kolmogorov scale. As a result, magnitudes of correction factors for the scalar dissipation rate are O(100).

A correction technique is demonstrated, which, for both turbulent energy and scalar dissipation estimates, assumes that behavior in the inertial range of scales follow theoretical predictions based on turbulent structure functions. Because this method relies on scales that should be independent of large-scale strain (e.g., that associated with velocity shear or density stratification), it is applicable to a wide range of flow fields. Additionally, while reliance on Kolmogorov's assumption of an inertial sub-range is explicit, the correction technique does not require an extensive inertial sub-range, so that energy and scalar dissipation rates in low-Re_λ flows may also be corrected. The proposed technique for estimating turbulent velocity and scalar dissipation rates has been demonstrated in turbulence with and without shear, and with and without density stratification.

It has also been demonstrated that the Karman–Howarth equality (and the analogous Yaglom equation for the scalar field) relating second- and third-order structure functions to dissipation rates is valid for both unstrained turbulence (decaying grid-generated turbulence), and density stratified and sheared turbulence at least up to the magnitudes of strains of the current experiments $Nt \sim 10$, $St \sim 10$, respectively. This is useful for it allows the use of these equations in the analysis of turbulence even when the large scale background profiles of velocity and scalar are unknown.

6 Appendix

The evolution equation for scalar variance ρ in tensor notation is given by:

$$\frac{\partial}{\partial t}\left(\frac{1}{2}\overline{\rho^2}\right) + U_k \frac{\partial}{\partial x_k}\left(\frac{1}{2}\overline{\rho^2}\right) = -\overline{\rho u_k}\frac{\partial \overline{\rho}}{\partial x_k} + \frac{\partial}{\partial x_k}\left(\frac{1}{2}\overline{\rho^2 u_k}\right) + D\frac{\partial^2}{\partial x_k^2}\left(\frac{1}{2}\overline{\rho^2}\right) - \overline{D\left(\frac{\partial \rho}{\partial x_k}\right)^2}$$

This represents a balance for ρ between the time rate of change, advection, gradient production, divergence, molecular diffusion, and scalar dissipation. For steady-state flow, neglect of divergence and molecular diffusion terms yields the simplified balance of Eq. 20 for shear-free, grid-generated turbulence (see Townsend 1980 for details and discussion).

References

Antonia RA, Chambers AJ (1980) On the correlation between turbulent velocity and temperature derivatives in the atmospheric surface layer. Bound Lay Meteorol 18:399–410

Antonia RA, Chambers AJ, Browne LWB (1983) Relations between structure functions of velocity and temperature in a turbulent jet. Exp Fluids 1:213–221

Antonia RA, Anselmet F, Chambers AJ (1986) Assessment of local isotropy using measurements in a turbulent plane jet. J Fluid Mech 163:365–391

Antonia RA, Zhu Y, Kim J (1993) On the measurement of lateral velocity derivatives in turbulent flows. Exp Fluids 15:65–69

Batchelor GK (1959) Small-scale variation of convected quantities like temperature in turbulent fluid. Part I. General discussion and the case of small conductivity. J Fluid Mech 5:113–133

Batchelor GK, Townsend AA (1948) Decay of isotropic turbulence in the initial period. Proc R Soc Lond A 193:539–558

Bershadskii A, Kit E, Tsinober A (1993) On universality of geometric invariants in turbulence—experimental results. Phys Fluids A 5(7):1523–1525

Comte-Bellot G, Corrsin S (1966) The use of a contraction to improve the isotropy of grid-generated turbulence. J Fluid Mech 25:657–682

Comte-Bellot G, Corrsin S (1971) Simple Eulerian time correlation of full- and narrow-band velocity signals in grid-generated, isotropic turbulence. J Fluid Mech 48:273–337

Danaila L, Anselmet F, Zhou T, Antonia RA (1999) A generalization of Yaglom's equation which accounts for the large-scale forcing in heated decaying turbulence. J Fluid Mech 391:359–372

Danaila L, Zhou T, Anselmet F, Antonia RA (2000) Calibration of a temperature dissipation probe in decaying grid turbulence. Exp Fluids 28:45–50

Dowling DR, Dimotakis PE (1990) Similarity of the concentration field of gas-phase turbulent jets. J Fluid Mech 218:109–141

Gargett A (1985) Evolution of scalar spectra with the decay of turbulence in a stratified fluid. J Fluid Mech 159:379–407

Gibson CH, Masiello PJ (1972) In: Rosenblatt M, Van Atta CW (eds) Statistical models and turbulence. Springer, Berlin Heidelberg New York

Gregg MC (1987) Diapycnal mixing in the thermocline: a review. J Geophys Res 92(C5):5249–5286

Harris VG, Graham JAH, Corrsin S (1977) Further experiments in nearly homogeneous turbulent shear flow. J Fluid Mech 81:657–687

Hinze JO (1975) Turbulence, 2nd edn. McGraw-Hill, New York

Huq P, Britter RE (1995a) Mixing due to grid-generated turbulence of a two-layer scalar profile. J Fluid Mech 285:17–40

Huq P, Britter RE (1995b) Turbulence evolution and mixing in a two-layer stably stratified fluid. J Fluid Mech 285:41–67

Itsweire EC, Helland KN, Van Atta CW (1986) The evolution of grid-generated turbulence in a stably stratified fluid. J Fluid Mech 162:299–338

Jayesh, Warhaft Z (1994) Turbulent penetration of a thermally stratified interfacial layer in a wind tunnel. J Fluid Mech 277:23–54

Jayesh, Tong C, Warhaft Z (1994) On temperature spectra in grid turbulence. Phys Fluids A 6:302–312

Kailasnath P, Sreenivasan KR (1993) Zero crossings of velocity fluctuations in turbulent boundary layers. Phys Fluids 5(11):2879–2885

King LV (1914) On the convection of heat from small cylinders in a stream of fluid: determination of the convection constants of small platinum wires with applications to hot-wire anemometry. Phil Trans R Soc A 214:373–432

Klebanoff PS (1954) Natl Adivsory Comm Aeronaut Technical Notes no 3178

Kolmogorov AN (1941a) The local structure of turbulence in incompressible viscous fluid for very large Reynolds numbers Dokl Akad Nauk SSSR 30(4):301–305, Reprinted in: Proc R Soc Lond A 434:9–13 (1991)

Kolmogorov AN (1941b) Dissipation of energy in the locally isotropic turbulence Dokl Akad Nauk SSSR 32(1):16–18, Reprinted in: Proc R Soc Lond A 434:15–17 (1991)

Kolmogorov AN (1962) A refinement of previous hypotheses concerning the local structure of turbulence in a viscous in-

compressible fluid at high Reynolds number. J Fluid Mech 13:82–85
Kraichnan RH (1968) Small-scale structure of a scalar field convected by turbulence. Phys Fluids 11:945–963
Lawson RE, Britter RE (1983) A note on the measurement of transverse fluctuations with heated cylindrical sensors at small mean velocities. J Phys E Sci Instrum 16:563–567
Ma B, Warhaft Z (1986) Some aspects of the thermal mixing layer in grid turbulence. Phys Fluids 29:3114–3120
Miller PL, Dimotakis PE (1996) Measurements of scalar power spectra in high Schmidt number turbulent jets. J Fluid Mech 308:129–146
Moisy F, Tabeling P, Willaime H (1999) Kolmogorov equation in a fully developed turbulence experiment. Phys Rev Lett 82:3994–3997
Monin AS, Yaglom AM (1971) Statistical fluid mechanics, mechanics of turbulence. MIT Press, Cambridge
Mydlarski L, Warhaft Z (1996) On the onset of high Reynolds number grid-generated wind tunnel turbulence. J Fluid Mech 320:331–368
Mydlarski L, Warhaft Z (1998) Passive scalar statistics in high-Peclet-number grid turbulence. J Fluid Mech 358:135–175
Nash JD, Moum JN (2002) Microstructure estimates of turbulent salinity flux and the dissipation spectrum of salinity. J Phys Oceanogr 32:2312–2333
Oakey N (1982) Determination of the rate of dissipation of turbulent energy from simultaneous temperature and velocity shear microstructure measurements. J Phys Oceanogr 12:256–271
Orlandi P, Antonia RA (2002) Dependence of the non-stationary form of Yaglom's equation on the Schmidt number. J Fluid Mech 451:99–108
Rohr JJ, Itsweire EC, Helland KN, Van Atta CW (1988) An investigation of the growth of turbulence in a uniform mean gradient shear flow. J Fluid Mech 187:1–33
Shah DA, Antonia RA (1986) Isotropic forms of vorticity and velocity structure function equations in several turbulent shear flows. Phys Fluids 29:4016–4024
Sreenivasan KR (1984) On the scaling of the turbulence energy dissipation rate. Phys Fluids 27(5):1048–1051
Sreenivasan KR (1998) An update on the energy dissipation rate in isotropic turbulence. Phys Fluids 10(2):528–529
Sreenivasan KR, Antonia RA, Danh HQ (1977) Temperature dissipation fluctuations in a turbulent boundary layer. Phys Fluids 20:1238–1249
Stillinger DC, Helland KN, Van Atta CW (1983) Experiments on the transition of homogeneous turbulence to internal waves in a stratified fluid. J Fluid Mech 131:91–122
Tavoularis S, Corrsin S (1981b) Experiments in nearly homogeneous turbulent shear flow with a uniform mean temperature gradient. Part 2. The fine structure. J Fluid Mech 104:349–367
Taylor GI (1938) Production and dissipation of vorticity in a turbulent fluid. Proc R Soc Lond A 164:15–23
Tennekes H, Lumley JL (1982) A first course in turbulence. MIT Press, Cambridge
Thoroddsen ST (1995) Reevaluation of the experimental support for the Kolmogorov refined similarity hypothesis. Phys Fluids 7(4):691–693
Thoroddsen ST, Van Atta CW (1996) Experiments on density-gradient anisotropies and scalar dissipation of turbulence in a stably stratified fluid. J Fluid Mech 322:383–409
Tong C, Warhaft Z (1994) On passive scalar derivative statistics in grid turbulence. Phys Fluids 6(6):2165–2176
Townsend AA (1980) The structure of turbulent shear flow. Cambridge University Press, Cambridge
Tsinober A (1993) Some properties of velocity derivatives in turbulent flows as obtained from experiments (laboratory and numerical). In turbulence in spatially extended systems. Nova Science Publishers Inc, New York, pp 117–128
Van Atta CW (1991) Local isotropy of the smallest scales of turbulent scalar and velocity fields. Proc R Soc Lond A 434:139–147
Von Kármán T, Howarth L (1938) On the statistical theory of isotropic turbulence. Proc R Soc Lond A 164:192–215
Warhaft Z (2000) Passive scalars in turbulent flows. Annu Rev Fluid Mech 32:203–240
Wyngaard JC (1971) The effect of velocity sensitivity on temperature derivative statistics in isotropic turbulence. J Fluid Mech 48:763–769
Yaglom AM (1949) On the local structure of a temperature field in a turbulent flow. Dokl Akad Nauk SSSR 69:743–746
Yamazaki H, Osborn T (1990) Dissipation estimates for stratified turbulence. J Geophys Res 95:9739–9744
Yoon K, Warhaft Z (1990) The evolution of grid-generated turbulence under conditions of stable thermal stratification. J Fluid Mech 215:601–638
Zhou T, Antonia RA (2000) Approximation for turbulent energy and temperature variance dissipation rates in grid turbulence. Phys Fluids 12(2):335–344